Reactive and Functional Polymers 169 (2021) 105065

Contents lists available at ScienceDirect

Reactive and Functional Polymers

journal homepage: www.elsevier.com/locate/react

Perspective Article

Organosoluble polyimides with low dielectric constant prepared from an asymmetric diamine containing bulky *m*-trifluoromethyl phenyl group

Min Zhong, Xiuming Wu, Chen Shu, Yuling Wang *, Xingyi Huang *, Wei Huang *

School of Chemistry and Chemical Engineering, State Key Laboratory of Metal Matrix Composites, Shanghai Key Laboratory of Electrical Insulation and Thermal Aging, Shanghai Jiao Tong University, 800 Dongchuan Road, Shanghai 200240, China

ARTICLE INFO

Keywords:
Low-*k*
Polyimide
Asymmetric diamine
m-Trifluoromethyl phenyl
Soluble

ABSTRACT

A series of polyimides (PIs) containing a bulky side group of *m*-trifluoromethyl phenyl was synthesized via a high-temperature one-step polycondensation of 4-[3′,5′-bis(trifluoromethyl)phenyl]-1,3-phenylenediamine (**2**) and various aromatic dianhydrides. The weight-averaged molecular weights (M_w) of the resulting PIs are between 3.92 and 8.36 × 10^4 g mol^{-1} with the M_w/M_n of 1.77–2.09. They are soluble in common organic solvents and easily processed into flexible films by the blade coating of PI solution. At room temperature, the dielectric constants (*k*) of these PI films are lower than 3.04 at 1 MHz and 2.87 at 10 GHz, especially the *k* of **2**-6FDA film is low to 2.66 at 1 MHz and 2.38 at 10 GHz. The breakdown strength of the resulting PI films (thickness: 10 ± 1 μm) is in the range from 461 to 523 kV mm^{-1}. Meanwhile, these PI films also show good thermal stability (5 wt% weight-loss temperature in the range of 521–571 °C under N_2; glass transition temperatures of 266–307 °C) and mechanical properties (tensile strength of 70.8–103.3 MPa, tensile modulus of 1.3–2.2 GPa, elongation at break of 9.1–10.8%). The average transmittance of these PI films (around 20 μm) is above 80% in the visible light region (400–760 nm). Such attractive comprehensive properties make these PIs as potential candidates for application in microelectronics industry.

1. Introduction

In recent years, more and more attention has been paid to low dielectric constant (low *k*) materials due to the urgent demand from microelectronics industry [1,2]. Low-*k* materials can reduce the resistance-capacitance delay, crosstalk noise and power dissipation, thus ensuring efficient operation of highly integrated circuits [3–7]. Polyimides are widely used in various fields of electronics, microelectronics, aerospace and energy on the base of their excellent thermal stability, mechanical strength and flexibility, solvent and chemical resistance, insulation and adhesion performances [8–12]. However, the relatively high *k* of traditional polyimides (e.g. Kapton PI films: *k* = 3.1–3.5) cannot meet the requirements of ultralarge-scale integration circuits and continuous miniaturization of electronic devices [13,14]. Nowadays, it is an urgent need to develop polyimides with lower dielectric constant as high-performance low *k* materials.

The one of most effective ways to reduce the *k* of PIs is the introduction of nano-sized air voids into them [15–19]. For example, Onodera et al. reported a porous PI film with the *k* values as low as 1.35 at 1 MHz when its porosity reached 86% [20]. However, the technique to prepare such porous PI films is complicated, difficult to control and expensive. In addition, the pore structure, size and distribution would greatly affect the homogeneity of PI films, which limited the large-area applications of this technique. On the other hand, the porosity would dramatically decrease the mechanical strength and toughness, enhance the moisture absorption and make them too fragile for practical uses [2,21]. Therefore, study on polyimides with the intrinsic low *k* is particularly significant for modern microelectronics industry.

The *k* of a polymer can be calculated according to Claslius-Mosotti equation [22,23]:

$$k = \frac{1 + 2(P_m/V_m)}{1 - (P_m/V_m)} \quad (1)$$

where P_m and V_m are the molar polarizability and the molar volume of atomic groups in a polymer, respectively. Obviously, the *k* value can be reduced by decreasing P_m or increasing V_m. Based on the above principle, the intrinsic low *k* polyimides can be obtained by introducing low polarizable fluorine substituents [24–27] or atomic groups with large volume into PI chains [28–31]. For instance, Zhang et al. reported a

* Corresponding authors.
E-mail addresses: wyl2005@sjtu.edu.cn (Y. Wang), xyhuang@sjtu.edu.cn (X. Huang), hw66@sjtu.edu.cn (W. Huang).

https://doi.org/10.1016/j.reactfunctpolym.2021.105065
Received 3 August 2021; Received in revised form 3 October 2021; Accepted 10 October 2021
Available online 12 October 2021

fluorinated polyimide with an ultralow k of 1.52 by introducing a rigid nonplanar conjugated side group [32]. However, the over complicated molecular design may greatly increase the cost of synthesis process and be difficult for industrialization [33]. As an alternative approach, the incorporation of asymmetric structure into a polyimide is also an efficient way to decrease its k [34,35], because the asymmetric structure can cause distortion, impede compact stacking and increase the free volume of PI chains.

In this work, we conveniently synthesized an asymmetric diamine **2** by introducing *m*-trifluoromethyl phenyl as pendant group via the Suzuki coupling reaction and then hydrogenation reaction. Then a series of PIs were prepared by the high-temperature one-step polycondensation from diamine **2** and various commercial aromatic dianhydrides. The resulting PIs were processed into films by the blade coating conveniently and further investigated by various measurements in detail. They could show intrinsic low k as well as excellent comprehensive properties.

2. Experimental

2.1. Materials

3,5-Bis(trifluoromethyl)benzeneboronic acid, 1-chloro-2,4-dinitrobenzene, Aliquat 336 (methyltrioctylammonium chloride), tetrakis(triphenylphosphine) palladium ($Pd(Pph_3)_4$), palladium 10% on carbon (10% Pd/C) and isoquinoline were purchased from Shanghai Titan Scientific Co., Ltd. Sodium carbonate anhydrous (Na_2CO_3), *o*-phthalic anhydride, pyridine, toluene and chloroform ($CHCl_3$) were purchased from Sinopharm Chemical Reagent Co., Ltd. Bis-(3-phthalyl anhydride) ether (ODPA, Adamas Reagent Co., Ltd), 3,3′,4,4′-biphenyltetracarboxylic dianhydride (BPDA, Aladdin Industrial Corporation) and 3,3′,4,4′-benzophenonetetracarboxylic dianhydride (BTDA, J&K Chemical Co., Ltd) were purified by recrystallization from acetic anhydride prior to use. 4,4′-(Hexafluoroisopropylidene) diphthalic anhydride (6FDA) was purchased from Zigong Zhongtiansheng New Material Technology Co., Ltd. *N*,*N*-dimethylacetamide (DMAc, Shanghai Titan Scientific Co., Ltd) and *m*-cresol (Shanghai Macklin Biochemical Co., Ltd) were purified by the vacuum distillation before use. All other solvents and reagents as analytical grade were purchased from Shanghai Titan Scientific Co., Ltd. and used without further treatment.

2.2. Measurements

All NMR spectra were recorded on a Bruker AVANCE III HD 500 spectrometer with $CDCl_3$ as solvents. Melting points (MP) of intermediate and diamine were measured by the polarized light micromelting point instrument (SWG X-4). Mass spectra were measured by Acquity UPLC & Q-TOF MS Premier and Bruker SolariX 7.0 T Fourier transform ion cyclotron resonance mass spectrometer (FT-ICRMS). Infrared spectra were recorded on a Perkin-Elmer Spectrum 100 Fourier transform infrared (FT-IR) spectrometer. Gel permeation chromatography (GPC) was performed with a Tosoh HLC-8320GPC analyzer (polystyrene calibration), using tetrahydrofuran (THF) as eluent with a flow rate of 1.0 mL min^{-1} at 40 °C. Elemental analysis was performed on a vario EL cube elemental analyzer. X-ray diffraction (XRD) patterns were obtained by a Bruker D8 advance X-ray diffractometer using Cu/Kα radiation with 2θ in the range from 5 to 50°. Thermogravimetric analyses (TGA) were performed with a TA Discovery TGA550 thermal analyzer with a heating rate of 20 °C min^{-1} from 50 to 800 °C under nitrogen. Differential scanning calorimetry (DSC) curves were obtained with a TA Discovery DSC 2500 thermal analyzer at a heating rate of 20 °C min^{-1} from 20 to 400 °C under flowing nitrogen. The thermal coefficient of expansion (CTE) values of PI specimens (15 mm long, 6 mm wide, and above 30 μm thick) were detected through thermomechanical analysis (TMA) on a Mettler Toledo TMA/SDTS841e thermal analyzer system under nitrogen at a heating rate of 10 °C min^{-1} from 50 to 200 °C with a 0.02 N expansion force. The mechanical property of the polyimide films was performed on an Instron 3365 materials testing system at a drawing speed of 1 mm min^{-1}. Ultraviolet-visible (UV–vis) transmittance spectra were recorded on a Perkin-Elmer Lambda 35 UV–vis spectrometer. The dielectric constant and dielectric loss were measured at frequency between 1 Hz and 1 MHz at 25 °C and 60% relative humidity, using a Novocontrol Concept 40 dielectric impedance spectrometer. The size of PI films was 20 mm × 20 mm × 35 μm and Platinum was vacuum-sprayed onto both surfaces of the samples to ensure excellent contact between the electrodes and the films. The dielectric constant and dielectric loss were also investigated at high frequency of 2 GHz and 10 GHz by a Keysight E5063A network analyzer at 25 °C. The size of PI films was π × 10 mm × 10 mm × 100 μm. The breakdown strength was measured by a DHV-60/2 DC high voltage generator. The applied voltage was increased at a rate of 200 V s^{-1} from 0 V until the breakdown occurring of a sudden current increase. Each sample (film thickness: 10 ± 1 μm) was kept in oil bath and repeatedly measured 10 times.

2.3. Synthesis of 4-[3′,5′-bis(trifluoromethyl)phenyl]-1,3-dinitrobenzene (1)

In a 1000 mL three-necked flask, 5.0638 g (25 mmol) 1-chloro-2,4-dinitrobenzene and 9.6722 g (37.5 mmol) 3,5-bis(trifluoromethyl)benzeneboronic acid were dissolved in 500 mL THF. Then, 90 mL 2 M aqueous Na_2CO_3 solution and 1.5 mL Aliquat 336 were added. The mixture was stirred for 45 min under nitrogen at room temperature. Subsequently, 1.1556 g (1 mmol) tetrakis(triphenylphosphine) palladium ($Pd(Pph_3)_4$) was added as a catalyst, and the reaction mixture was stirred at 90 °C for 12 h. After removing the aqueous layer, the organic layer was concentrated, dissolved with dichloromethane, and washed with deionized water for three times, then black solid was obtained by rotary evaporation. The resulting solid was further purified by silica gel column chromatography using dichloromethane/petroleum ether (v/v = 1/2) and recrystallization in toluene to obtain some orange blocky crystal **1**, 7.8417 g. Yield: 82.5%; MP: 113.6–116.1 °C; ^{1}H NMR (500 MHz, $CDCl_3$) δ 8.92 (d, J = 2.1 Hz, 1H), 8.57 (dd, J = 8.4, 2.3 Hz, 1H), 8.02 (s, 1H), 7.79 (s, 2H), 7.71 (d, J = 8.4 Hz, 1H); ^{13}C NMR (126 MHz, $CDCl_3$) δ 148.62, 148.17, 139.56, 137.94, 133.67, 132.66 (q, J = 34.0 Hz), 128.22, 127.47, 123.42, 122.95 (q, J = 273.5 Hz), 120.59; HRMS (MALDI, m/z): $[M\text{-}H]^-$ calculated for $C_{14}H_5F_6N_2O_4^-$, 379.0159; found, 379.0159.

2.4. Synthesis of 4-[3′,5′-bis(trifluoromethyl)phenyl]-1,3-phenylenediamine (2)

30.4162 g (80 mmol) purified dinitro compound **1**, 0.3725 g 10% Pd/C catalyst, and 60 mL ethanol were added into a flame-dried pressure reactor. Hydrogenation was carried out at 50 °C under a hydrogen pressure of 7 MPa for 24 h. After cooling to room temperature, the mixture was filtered to remove the Pd/C catalyst. Then, the solution was dried by rotary evaporation, resulting in an orange solid crude product. Under the protection of nitrogen, the crude product was recrystallized from ethanol for three times to afford yellow aciculate crystal **2**, 19.2143 g. Yield: 75%; MP: 154.1–154.9 °C; ^{1}H NMR (500 MHz, $CDCl_3$) δ 7.91 (s, 2H), 7.78 (s, 1H), 6.93 (d, J = 8.1 Hz, 1H), 6.23 (dd, J = 8.1, 2.2 Hz, 1H), 6.12 (d, J = 2.2 Hz, 1H), 3.71 (s, 2H), 3.65 (s, 2H); ^{13}C NMR (126 MHz, $CDCl_3$) δ 148.26, 144.50, 142.13, 132.05 (q, J = 33.1 Hz), 131.76, 129.31, 123.54 (q, J = 273.2 Hz), 120.18, 115.63, 106.93, 102.08; HRMS (ESI, m/z): $[M + H]^+$ calculated for $C_{14}H_{11}F_6N_2^+$, 321.0821; found, 321.0840.

2.5. Synthesis of model compound (MC)

0.1601 g (0.5 mmol) diamine **2**, 0.3703 g (2.5 mmol) *o*-phthalic anhydride, and 5 mL DMAc were added into a 100 mL three-necked flask. Under N_2 atmosphere, the mixture was stirred at room

temperature for 24 h and 50 °C for 24 h. After cooling to room temperature, 0.2042 g (2 mmol) acetic anhydride and 0.0791 g (1 mmol) pyridine were added. The mixture was then stirred at room temperature for 12 h and 60 °C for 3 h. Subsequently, the solution was precipitated in water. White powdery solid was collected by filtration and then washed with hot water several times. The resulted solid was further purified by silica gel column chromatography using ethyl acetate/petroleum ether (*v*/v = 1/1). Yield: 85%; ^{1}H NMR (500 MHz, $CDCl_3$) δ 8.01–7.97 (m, 2H), 7.87–7.81 (m, 5H), 7.78 (s, 2H), 7.76 (s, 1H), 7.75–7.67 (m, 4H); HRMS (MALDI, *m/z*): $[M + Na]^+$ calculated for $C_{30}H_{14}F_6N_2O_4Na^+$, 603.0750; found, 603.0733.

2.6. Synthesis of PIs

All the PIs were synthesized by the high-temperature one-step polycondensation. As a typical example, **2**-6FDA was synthesized according to the following procedure. 0.4996 g (1.56 mmol) **2**, 0.6930 g (1.56 mmol) 6FDA, 6.5 mL *m*-cresol, and five drops isoquinoline were added into a 100 mL three-necked flask. Under N_2 atmosphere, the mixture was firstly stirred at room temperature for 2 h and subsequently heated with the following temperature program of 50 °C for 12 h, 80 °C for 12 h, 100 °C for 12 h, 150 °C for 4 h, 180 °C for 4 h and 200 °C for 4 h. After cooling to room temperature, 3 mL chloroform was added into the viscous mixture. Then the mixture was poured slowly into 400 mL methanol under the vigorous stirring to produce some pale-yellow fiber-like precipitate. **2**-6FDA was collected by filtration and dried in vacuum at 100 °C for 24 h. The polyimide was purified by reprecipitating twice.

2-6FDA: Yield: 94%. FT-IR (film, cm^{-1}): ν = 1789 (C=O), 1738 (C=O), 1621, 1515, 1385 (C-N), 1280, 1140, 1107, 902, 827, 712, 632. ^{1}H NMR (500 MHz, $CDCl_3$) δ 8.08–7.78 (m, 6H), 7.81 (s, 1H), 7.80 (s, 1H), 7.74 (s, 2H), 7.72 (d, *J* = 8.4 Hz, 1H), 7.67 (s, 1H).

2-ODPA: Yield: 97%. FT-IR (film, cm^{-1}): ν = 1785 (C=O), 1730 (C=O), 1610, 1514, 1385 (C-N), 1279, 1136, 1096, 901, 827, 709, 629. ^{1}H NMR (500 MHz, $CDCl_3$) δ 8.04–7.86 (m, 2H), 7.83 (d, *J* = 8.25 Hz, 1H), 7.79 (d, *J* = 7.15 Hz, 1H), 7.77 (s, 2H), 7.69 (s, 1H), 7.68 (s, 1H), 7.60–7.34 (m, 4H).

2-BPDA: Yield: 95%. FT-IR (film, cm^{-1}): ν = 1780 (C=O), 1730 (C=O), 1619, 1514, 1384 (C-N), 1279, 1136, 1099, 901, 826, 709, 630. ^{1}H NMR (500 MHz, $CDCl_3$) δ 8.29–7.92 (m, 6H), 7.88 (s, 1H), 7.84–7.74 (m, 4H), 7.71 (s, 1H).

2-BTDA: Yield: 97%. FT-IR (film, cm^{-1}): ν = 1784 (C=O), 1732 (C=O), 1616, 1514, 1384 (C-N), 1280, 1137, 1099, 902, 826, 710, 631. ^{1}H NMR (500 MHz, $CDCl_3$) δ 8.33–7.92 (m, 6H), 7.84 (s, 1H), 7.76 (s, 3H), 7.71 (s, 2H).

2.7. Film preparation

All the PI films were prepared by the blade coating of PI solution. As a typical example, the preparation of **2**-6FDA film was carried out as follows: 0.6 g **2**-6FDA was dissolved in 4 mL DMAc completely and kept at 60 °C for 12 h. Then the solution was filtered by a 0.7 μm fiberglass syringe filter and blade-coated on a clean dry glass substrate at 60 °C by using an Elcometer 4340 Automatic Film Applicator. The blade height was 800 μm and the coating speed was 0.2 in. s^{-1}. The glass substrate with PI solution was kept 60 °C overnight to evaporate the solvent, and then dried under vacuum at 80 °C for 12 h, 100 °C for 12 h and 200 °C for 24 h to remove the residual solvent. After cooling to room temperature, the PI film was peeled off the glass substrate by soaking in deionized water.

3. Results and discussion

3.1. Synthesis and characterization of diamine 2

As shown in Scheme 1, diamine **2** with a pedant bulky group of *m*-trifluoromethyl phenyl was synthesized from 1-chloro-2,4-dinitrobenzene and 3,5-bis(trifluoromethyl)benzeneboronic acid via Suzuki coupling reaction and then hydrogenation reaction.

The chemical structures of dinitro-intermediate **1** and diamine **2** were confirmed by ^{1}H NMR spectra, ^{13}C NMR spectra and mass spectra. The ^{1}H and ^{13}C NMR spectra of dinitro-intermediate **1** and diamine **2** were shown in Figs. 1 and 2, respectively. All the signals were labelled and accurately ascribed to the corresponding protons or carbon atoms in dinitro-intermediate **1** and diamine **2**. When dinitro-intermediate **1** was transformed into diamine **2** by hydrogenation, some new signals were appeared at 3.65–3.71 ppm in ^{1}H NMR spectrum of diamine **2**, which was belong to the protons of amino-groups. Due to the asymmetric molecular structure of diamine **2**, these signals presented as partially overlapping saddle-shaped peaks. In addition, the signals of both carbon atom 9 and 10 were split into quadruple peaks in the ^{13}C NMR spectra of dinitro-intermediate **1** and diamine **2**, which was attributed to the influence of fluorine atoms in trifluoromethyl groups. The melting points of dinitro-intermediate **1** and diamine **2** were 113.6–116.1 °C and 154.1–154.9 °C respectively, measured by the polarized light micro-melting point instrument. All above experimental data confirmed the expected chemical structures of dinitro-intermediate **1** and diamine **2**.

3.2. Synthesis and characterization of PIs

As shown in Scheme 2, all the PIs were prepared by the high-temperature one-step polycondensation of diamine **2** with various

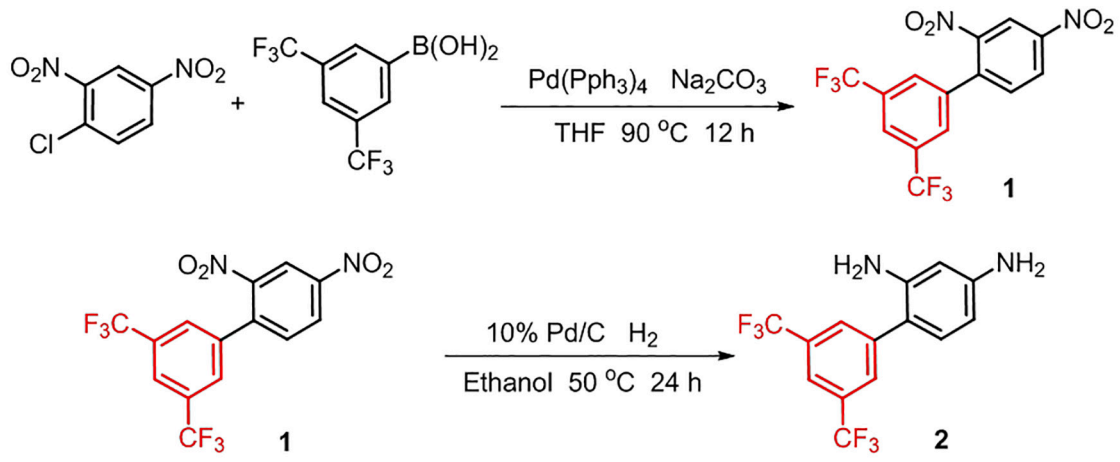

Scheme 1. Synthesis route of diamine **2**.

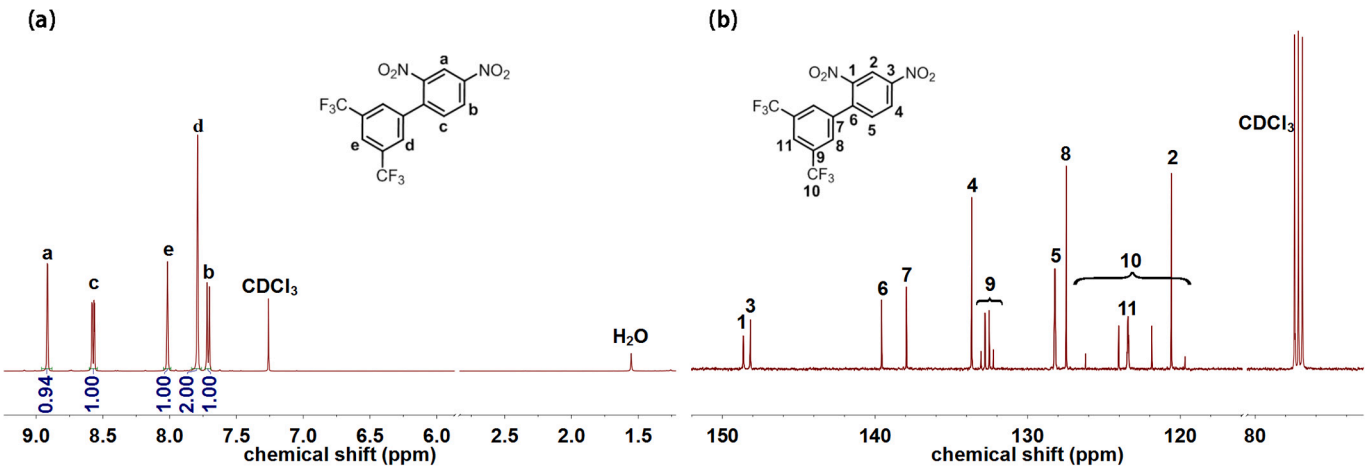

Fig. 1. (a) ^{1}H and (b) ^{13}C NMR spectra of dinitro-intermediate **1** in $CDCl_3$.

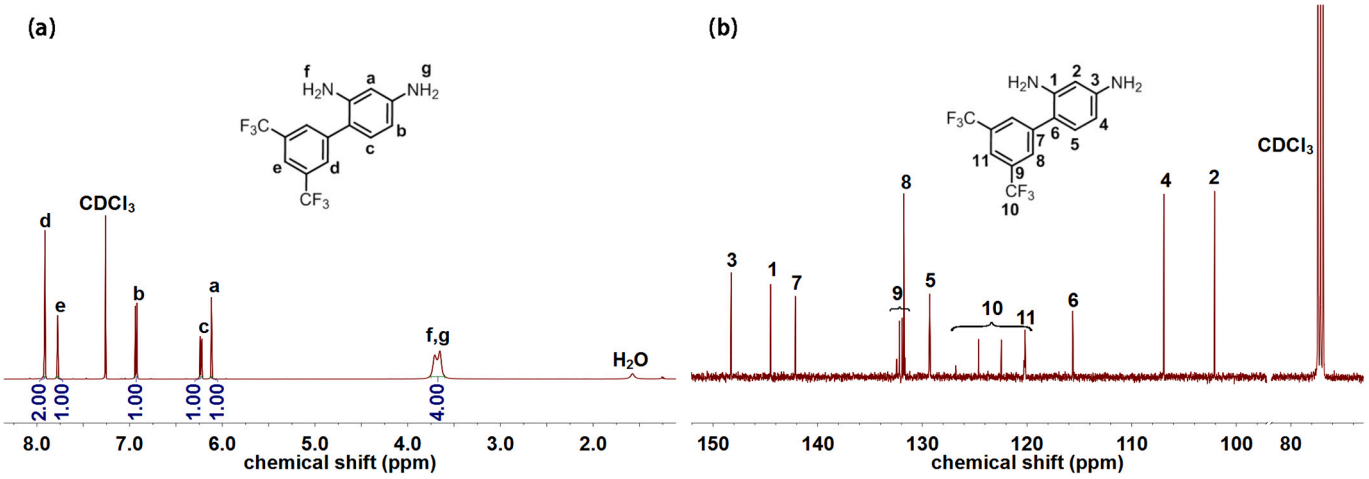

Fig. 2. (a) ^{1}H and (b) ^{13}C NMR spectra of diamine **2** in $CDCl_3$.

aromatic dianhydrides (including 6FDA, ODPA, BPDA and BTDA) in *m*-cresol at the solid content of 15 wt% with isoquinoline as a catalyst.

The FT-IR spectra of the resulting PIs were exhibited in Fig. 3. The characteristic absorption peaks of the imide group at 1780–1789 cm^{-1} (C=O asymmetrical stretching), 1730–1738 cm^{-1} (C=O symmetrical stretching) and 1384–1385 cm^{-1} (C-N asymmetrical stretching) were observed clearly, while the characteristic absorption peaks of amino groups in the range from 3400 to 3500 cm^{-1} were almost disappeared completely. Except for the bands at 3070–3080 cm^{-1} (aromatic C-H stretching vibrations), no obvious peaks of amide groups were observed in the region between 3220 and 3440 cm^{-1} (N-H stretching) [3,36,37]. All above results indicated the nearly full imidization of the resulting PIs.

The chemical structures of the resulting PIs were characterized by ^{1}H NMR measurement. As a typical example, the ^{1}H NMR spectrum of **2**-6FDA was shown in Fig. 4b. Unfortunately, it is hard to assign all the peaks of **2**-6FDA directly due to the introduction of asymmetrical *m*-trifluoromethyl phenyl adding the complexity of its ^{1}H NMR spectrum. Thus, we synthesized a model compound and simultaneously 2D ^{1}H-^{1}H COSY NMR measurement was adopted to analyze the ^{1}H NMR spectra of the resulting PIs. Comparing with the ^{1}H NMR spectrum of diamine **2** (Fig. 2) and combining the 2D ^{1}H-^{1}H COSY NMR spectrum of **MC**, the chemical shifts of H_d and H_e in the benzene ring of *m*-trifluoromethyl phenyl of **MC** are similar, but the chemical shifts of H_a, H_b and H_c in the benzene ring containing amino groups of **MC** are shifted to 7.8–8.0 ppm from 6.0–7.0 ppm, which can be ascribed to the great chemical environment changes resulting from the conversion of amino groups to phthalimides. On the other hand, the peaks of H_f, H_g, H_h and H_i in the benzene ring of phthalimides appear at the different chemical shift position because of the asymmetrical structure in diamine unit (Fig. 4a). According to the above results and combining the 2D ^{1}H-^{1}H COSY NMR spectrum of **2**-6FDA, the peaks at 7.6–7.9 ppm can be attributed to the protons of H_a - H_e in the diamine unit of **2**-6FDA. Correspondingly, the peaks of the protons (H_f, H_g, H_h) in dianhydride unit of **2**-6FDA present as complicated multiple peaks, which is attributed to the influence of the asymmetric structure of diamine unit. Fortunately, 2D ^{1}H-^{1}H COSY NMR spectrum of **2**-6FDA demonstrated the correlation between the proton peaks (H_a, H_b, H_c) in diamine unit and those (H_f, H_g, H_h) in dianhydride unit, which helped us to assign all the peaks to the corresponding protons. All above data confirmed the chemical structure of **2**-6FDA. The ^{1}H and ^{1}H-^{1}H COSY NMR spectra of other PIs were shown in Figs. S1 - S3 of Supporting Information and all the peaks were assigned to the corresponding protons, which confirmed their chemical structure well.

The elemental analysis data of the resulting PIs were exhibited in Table 1. Obviously, the experimental results were in accordance with the corresponding theoretical values and further confirmed the chemical structures of the resulting PIs.

3.3. Solubility

Generally, the solubility of polymers is mainly determined by two key factors, i.e. chain packing ability and intermolecular interaction

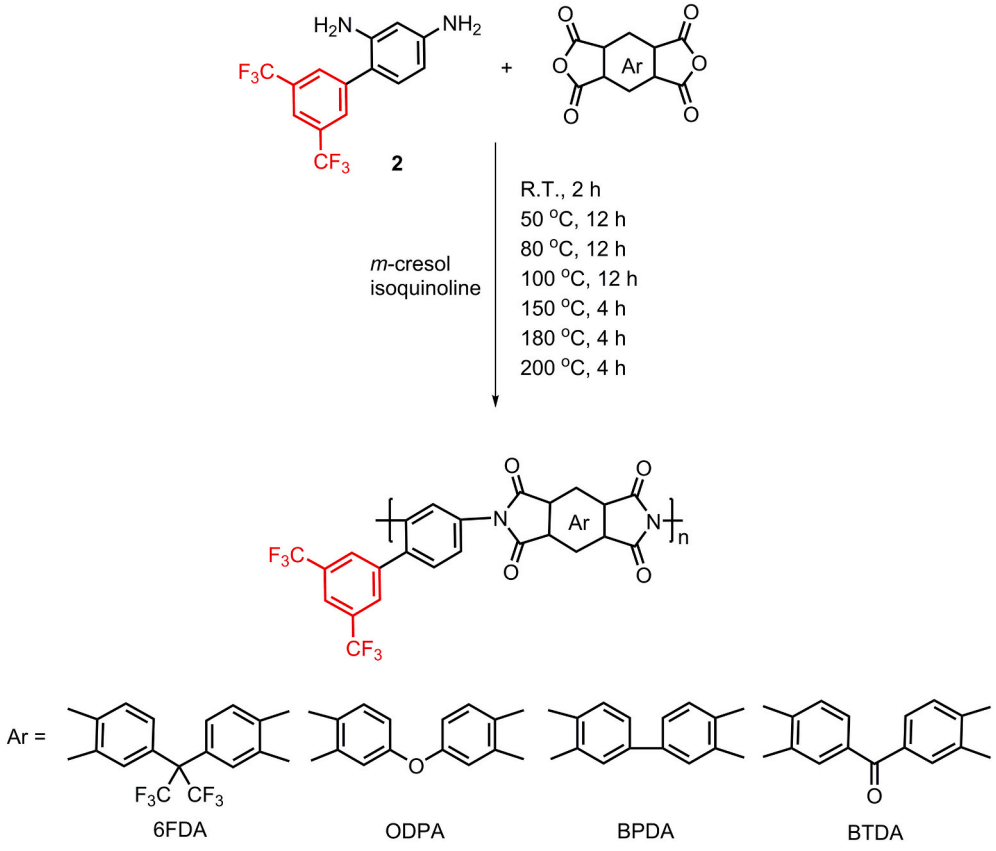

Scheme 2. Synthesis route of PIs.

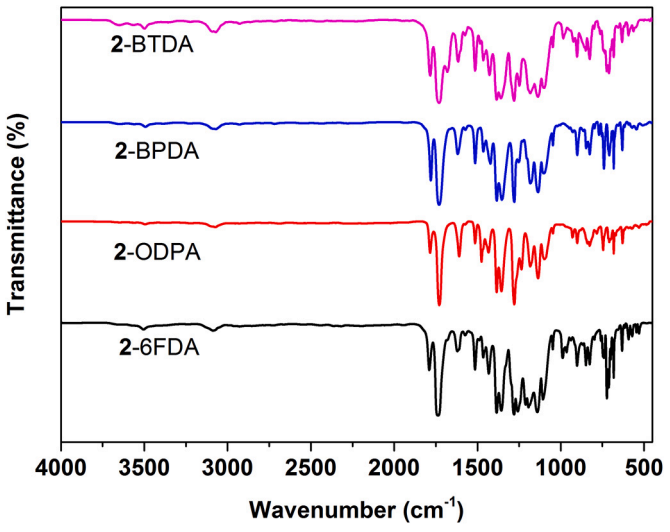

Fig. 3. FT-IR spectra of PIs.

[38]. The solubility of the PIs was investigated and summarized in Table 2. All the PIs are soluble in common polar organic solvents (e.g. *N*-methylpyrrolidone (NMP), DMAc, dimethylformamide (DMF), dimethyl sulfoxide (DMSO)), and even in low boiling organic solvents (e.g. THF and chloroform). This can be attributed to the steric hindrance effect of the pendant bulky *m*-trifluoromethyl phenyl groups, which improves the distance between the PI chains and decreases intermolecular interaction to promote the penetration of solvent. Especially, **2**-6FDA is even soluble in acetone at 25 °C. This can be attributed to large volume and high electronegativity of hexafluoro-isopropyl in 6FDA, which further inhibit the close packing of PI chains. On the contrary, **2**-BPDA cannot dissolve in acetone at 25 °C due to the rigid biphenyl structure of BPDA. In summary, the excellent solubility is beneficial for the continuous roll-to-roll process of PIs for practical applications.

The molecular weights of the resulting PIs were determined by GPC and the data were summarized in Table 2. The weight-averaged molecular weights of the resulting PIs are in the range from 3.92×10^4 to 8.36×10^4 with the M_w/M_n from 1.77 to 2.09. So they can be processed into flexible films by the blade coating of solutions.

3.4. Morphology

The morphology of the resulting PI films was analyzed by XRD measurement and the results were shown in Fig. 5. No sharp melt peak of crystallization was observed in their XRD curves, which indicated they were amorphous [39]. The broad diffuse peaks from 13.51° to 13.66° represent the average interchain *d*-spacing, which reflects the chain packing efficiency of PIs [40]. The shoulder peaks ranging from 25° to 35° can be assigned to the π-π stacking of imide and phenyl rings [41,42]. The corresponding *d*-spacing (calculated according to Bragg equation: $n\lambda = 2d\sin\theta$) of them was in the sequence of **2**-BPDA (6.48 Å) < **2**-BTDA (6.52 Å) < **2**-ODPA (6.53 Å) < **2**-6FDA (6.55 Å). The *d*-spacing difference among them can be ascribed to different dianhydride units. For example, the bulky hexafluoro-isopropyl with high electronegativity in 6FDA endows the large free volume and averaged interchain distance for **2**-6FDA and the flexible ether linkage in ODPA is beneficial for the rotation of phenyl rings for **2**-ODPA, both of which reduce the close packing of PI chains and increase the *d*-spacing comparing with the rigid biphenyl in BPDA for **2**-BPDA [42,43]. All the *d*-spacings of them are larger than that of Kapton film (4.78 Å) [44]. This can be attributed to the introduction of pendant bulky *m*-trifluoromethyl phenyl to effectively hinder the close stacking of PI chains and restrict

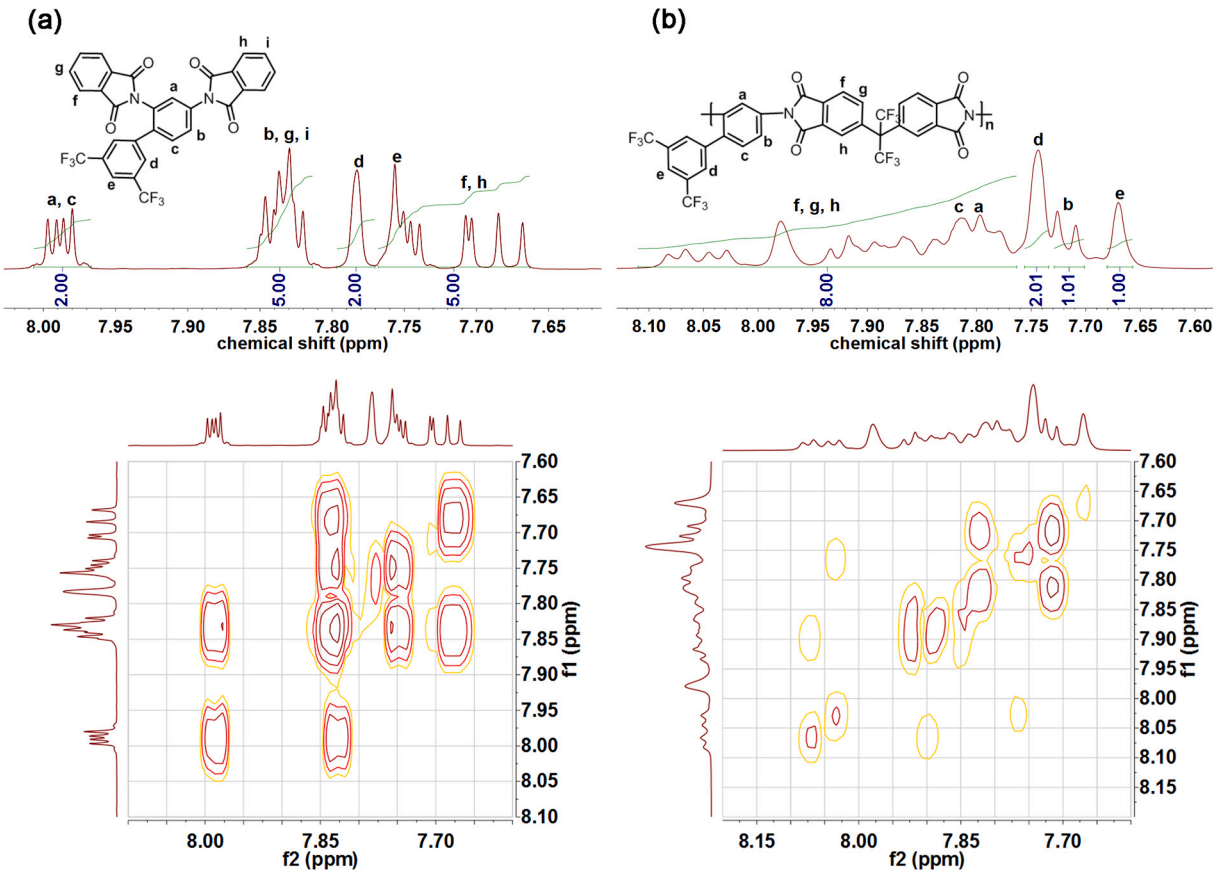

Fig. 4. ^{1}H and ^{1}H-^{1}H COSY NMR spectra of (a) **MC** and (b) **2**-6FDA in $CDCl_3$.

Table 1
Elemental analysis data of PIs.

PIs	Formula		C	H	N
2-6FDA	$C_{33}H_{12}F_{12}N_2O_4$	Calculated	54.41	1.66	3.85
		Found	54.46	1.65	3.91
2-ODPA	$C_{30}H_{12}F_6N_2O_5$	Calculated	60.62	2.03	4.71
		Found	60.52	2.01	4.75
2-BPDA	$C_{30}H_{12}F_6N_2O_4$	Calculated	62.29	2.09	4.84
		Found	61.93	2.14	4.81
2-BTDA	$C_{31}H_{12}F_6N_2O_5$	Calculated	61.40	1.99	4.62
		Found	61.57	2.08	4.49

the formation of ordered structure.

3.5. Thermal properties

The thermal properties of the resulting PIs were investigated by TGA, DSC and TMA measurements. The TGA and DSC curves were displayed in Fig. 6 and other key data were summarized in Table 3. According to the TGA analyses, all the resulting PIs have outstanding thermal stability with negligible weight loss up to 500 °C in nitrogen, which allows them to undergo the relatively high temperature of processing and application required for microelectronics industry. The 5 wt% and 10 wt% weight-loss temperatures of them in nitrogen were in the range of 521–571 °C and 541–592 °C, respectively. Besides, the char yields of these PIs were more than 38% at 800 °C in nitrogen. Especially, **2**-6FDA with the highest content of fluorine showed the highest char yield due to the high bonding energy of C-F bond [45,46]. In addition, **2**-ODPA possessed the lowest glass transition temperature (T_g) of 266 °C and the largest CTE value of 61 ppm $^{o}C^{-1}$ due to the flexible ether linkage in ODPA, while **2**-BPDA had the highest T_g of 307 °C and the lowest CTE value of 42 ppm $^{o}C^{-1}$ on the base of the rigid biphenyl structure in BPDA. No endothermic peak above the T_g was observed on the DSC curves and also indicated the amorphous structure of the PI films, which was in accordance with the XRD results.

Table 2
Molecular weights and solubility of PIs.

	GPC		Solubility[a]						
PIs	M_w[b] $\times 10^{-4}$	M_w/M_n[c]	NMP	DMAc	DMF	THF	$CHCl_3$	DMSO	Acetone
2-6FDA	6.99	1.79	++	++	++	++	++	+	++
2-ODPA	6.04	1.77	++	++	++	++	++	++	+−
2-BPDA	3.92	1.89	++	++	++	++	++	+	−
2-BTDA	8.36	2.09	++	++	++	++	++	++	+−

[a] Solubility: ++, soluble at 25 °C; +, partially soluble at 25 °C and soluble on heating; +−, swelling; −, insoluble even on heating. The solubility was determined by adding 2 mg PI into 1 mL solvent.
[b] M_w: weight-averaged molecular weight.
[c] M_n: number-averaged molecular weight.

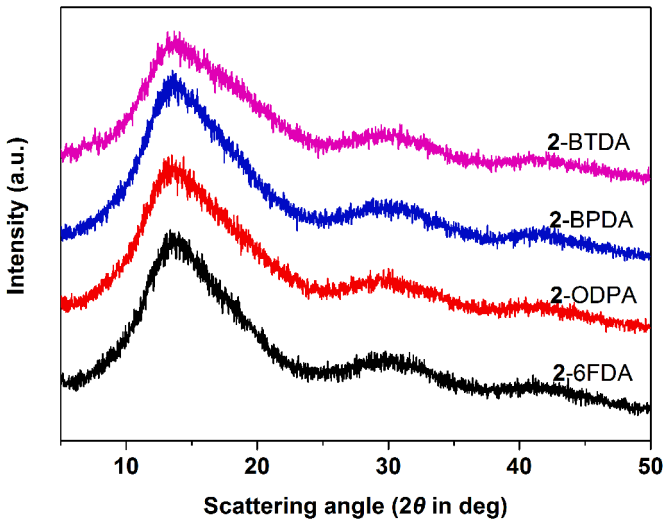

Fig. 5. XRD curves of PI films.

3.6. Mechanical properties

The mechanical properties of the PI films were investigated by tensile tests at room temperature and the results with the corresponding film thickness were listed in Table 4. The tensile strength and tensile modulus of them were in the range of 70.8–103.3 MPa and 1.3–2.2 GPa respectively, with the elongation at break in the range from 9.1% to 10.8%, which suggested the tough and flexible PI films (Fig. 7) could be obtained with the blade coating of PI solutions on glass plate in the laboratory.

3.7. Optical properties

According to previous reports, the deep color of conventional aromatic PIs was mainly attributed to the strong light absorption in the UV–visible range caused by the formation of intramolecular and intermolecular charge transfer complexes (CTC) between the electron-donating diamine and electron-accepting aromatic dianhydride [47]. Here the incorporation of the pendant bulky *m*-trifluoromethyl phenyl increased the intermolecular distance to inhibit the formation of CTC, which resulted in the good optical properties of them. The UV–vis spectra of the resulting PI films (thickness: 20 ± 1 μm) were shown in Fig. 8 and the corresponding data were summarized in Table 5. These films showed better optical properties (cut-off wavelength $\lambda_0 \leq 380$ nm, average transmittance in the visible light range $T_{vis} > 80\%$) than those of Kapton film ($\lambda_0 = 400$ nm, $T_{vis} = 69\%$) [48].

Among them, **2**-6FDA film is the most transparent one with the lowest cut-off wavelength of 326 nm and the highest T_{vis} of 89% and T_{400} of 79%. The hexafluoro-isopropyl in 6FDA provides the steric hindrance and low polarizability of C-F bonds to inhibit the formation of CTC [49,50]. **2**-ODPA film is also the better transparent one with the cut-off wavelength of 354 nm and the T_{vis} of 86% and T_{400} of 72%. The flexible ether linkage in ODPA weakens the intramolecular conjugation

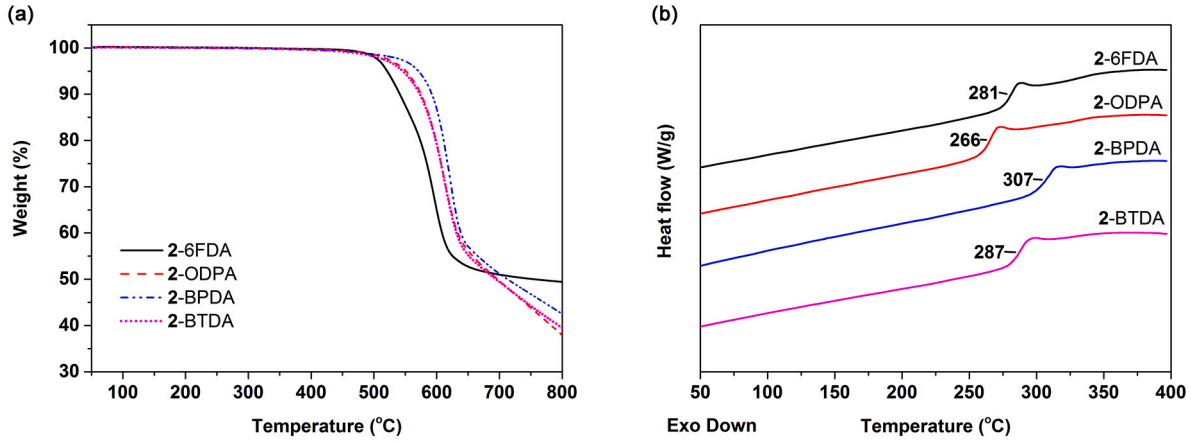

Fig. 6. (a) TGA and (b) DSC curves of PIs.

Table 3
Thermal properties of PIs.

PIs	T_g (°C)	$T_{5\ wt\%}$ (°C)	$T_{10\ wt\%}$ (°C)	Char yield[a] (wt%)	CTE (ppm $^{o}C^{-1}$)
2-6FDA	281	521	541	49	58
2-ODPA	266	551	575	38	61
2-BPDA	307	571	592	43	42
2-BTDA	287	546	573	40	54

[a] Residual weight percentage at 800 °C in nitrogen.

Table 4
Mechanical behaviors of PI films.

PIs	Film thickness (μm)	Tensile strength (MPa)	Tensile modulus (GPa)	Elongation at break (%)
2-6FDA	38	70.8	1.3	9.6
2-ODPA	36	99.0	1.6	9.6
2-BPDA	45	103.3	2.2	10.8
2-BTDA	36	89.5	1.5	9.1

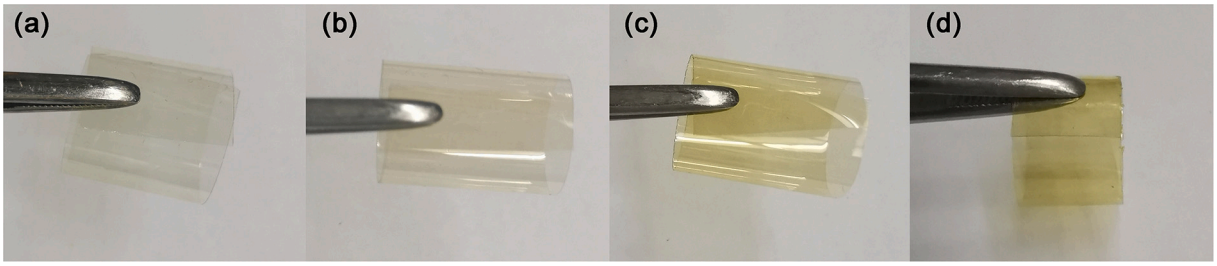

Fig. 7. Photographs of PI films (a) **2**-6FDA, (b) **2**-ODPA, (c) **2**-BPDA and (d) **2**-BTDA.

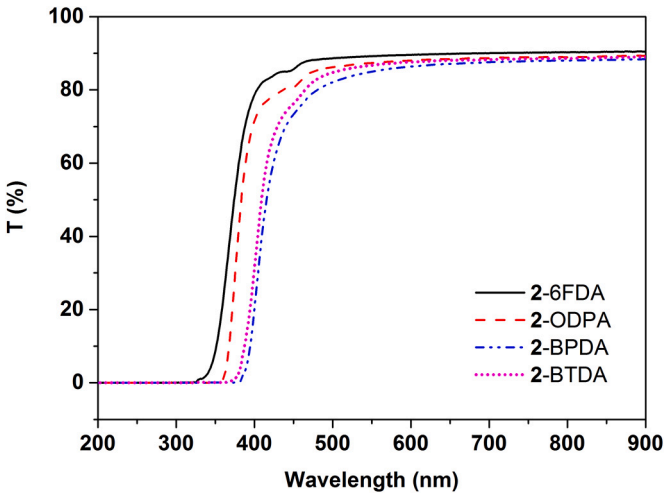

Fig. 8. UV–vis spectra of PI films (thickness: 20 ± 1 μm).

Table 5
Optical properties of PI films.

PIs	Film thickness (μm)	T_{vis} [a] (%)	T_{400} [b] (%)	λ_0 [c] (nm)
2-6FDA	20	89	79	326
2-ODPA	21	86	72	354
2-BPDA	19	81	20	380
2-BTDA	20	83	31	369

[a] The average transmittance in the visible light range (400–760 nm).
[b] Transmittance at 400 nm.
[c] UV cut-off wavelength.

and CTC effect [48]. Instead, **2**-BPDA film displayed the lowest T_{vis} of 81% and T_{400} of 20% due to its close packing of polymer chains and the relatively enhanced CTC effect. Its cut-off wavelength was red-shifted to 380 nm due to the more planar structure and higher degree of conjugation [51]. **2**-BTDA film also possessed the relatively lower T_{400} of 31% and higher cut-off wavelength of 369 nm, which was attributed to the electron withdrawing group carbonyl between two phenyls in BTDA to increase the intramolecular CTC and decrease its transparency [52]. The higher cut-off wavelengths of **2**-BPDA and **2**-BTDA films are also coincident with their deeper color observed in Fig. 7 [53].

3.8. Dielectric properties

The dielectric constant and dielectric loss of the PI films were studied at frequencies between 1 Hz and 1 MHz at 25 °C and 60% relative humidity using a Novocontrol Concept 40 dielectric impedance spectrometer. The curves of dielectric constant and dielectric loss as a function of frequency were shown in Fig. 9 and the corresponding values were listed in Table 6. The dielectric constant of the PI films gradually decreases in different level with the increase of the frequency. This is because the orientation of polarizable units is fast enough with the oscillations of the alternative electric field at low frequency, but at high frequency the dipole no longer follows the oscillations of the external field, which results in reducing the polarization and the dielectric constant [54]. The dielectric loss of the PI films almost increases with the increase of the frequency. This is because the forced movement occurs after the orientation lag of the dipole at the high frequency, which brings in an increase of energy loss of the electric field. The dielectric loss of **2**-6FDA film is an exceptional, which decreases at the low frequency ($< 10^3$ Hz) and then increases at the high frequency ($> 10^4$ Hz) with the frequency increasing. This can be attributed to the different secondary relaxation processes including γ and β relaxation [54]. Similar phenomena were also observed in other 6FDA-derived PI films according to previous reports [30,55,56].

In comparison with Kapton film ($k = 3.1$–3.5) [13], the resulting PI films displayed lower dielectric constant in the range from 2.66 to 3.04 at 1 MHz. The decreased dielectric constant might be attributed to the introduction of the pendant bulky asymmetric *m*-trifluoromethyl phenyl, which prevented the tight packing of PI chains and increased their free volume. In addition, the strong electronegativity of fluorine results in very low polarizability of the C-F bonds, which decreases the total polarizability of the polymer and can further reduce the dielectric constant [57]. Hence, **2**-6FDA film with the highest content of fluorine in the repeat unit possessed the lowest dielectric constant at low frequency. The dielectric constants of other three PI films were relatively high with slight difference. Such slight difference was attributed to the different chemical structure of dianhydride unit among them. The dielectric loss of these PI films was increased with the frequency increasing. The dielectric constant and dielectric loss of the PI films at high frequency of 2 GHz and 10 GHz were listed in Table 7. Obviously, the dielectric constant of each PI film at high frequency (GHz) is lower than the corresponding one at low frequency (MHz) due to the reduced polarization. **2**-6FDA film also exhibited the lowest dielectric constant of 2.38 at high frequency of 10 GHz. The dielectric loss of each PI film at high frequency is also lower than the corresponding one at 1 MHz.

Breakdown strength is defined as the ratio of the breakdown voltage to the dielectric thickness and it determines the operating electric field of a particular dielectric material [58]. The breakdown strength of the resulting PI films was tested under direct current at room temperature and the two-parameter Weibull distribution function [59] was employed to conduct the statistical analysis:

$$P = 1 - exp\left[-\left(\frac{E}{\alpha}\right)^{\beta}\right] \quad (2)$$

where P is the probability of failure at an electric field up to E; E is the experimental breakdown strength; α is the scale parameter referring to the breakdown strength with a 63.2% probability of failure; and β is the shape parameter, which is a measure of dispersion in the data. Eq. (2) can be written as below by taking two logarithms:

$$ln(-ln(1-P)) = \beta lnE - \beta ln\alpha \quad (3)$$

The Weibull distribution fitting curves were presented in Fig. S4 and

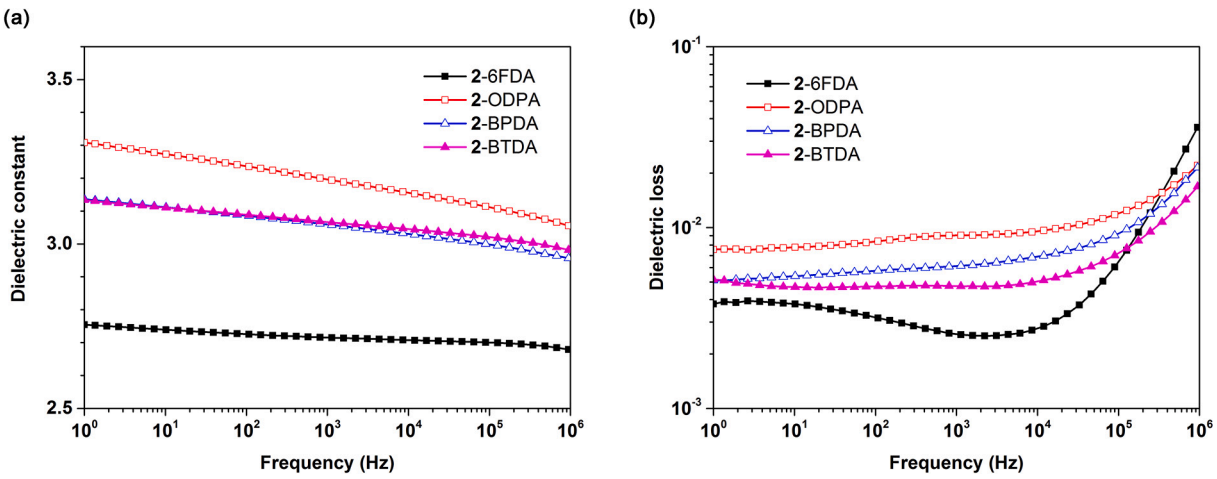

Fig. 9. (a) Dielectric constant and (b) dielectric loss as a function of frequency for PI films.

Table 6
Dielectric properties of PI films at low frequency.

PIs	Dielectric constant			Dielectric loss			Breakdown strength (kV mm^{-1})
	1 kHz	10 kHz	1 MHz	1 kHz	10 kHz	1 MHz	
2-6FDA	2.71	2.70	2.66	0.0025	0.0028	0.0431	523
2-ODPA	3.19	3.15	3.04	0.0090	0.0096	0.0253	518
2-BPDA	3.05	3.02	2.94	0.0061	0.0069	0.0261	461
2-BTDA	3.06	3.04	2.97	0.0047	0.0051	0.0195	479

Table 7
Dielectric properties of PI films at high frequency.

PIs	Dielectric constant		Dielectric loss	
	2 GHz	10 GHz	2 GHz	10 GHz
2-6FDA	2.40	2.38	0.0064	0.0082
2-ODPA	2.83	2.80	0.0082	0.0110
2-BPDA	2.91	2.87	0.0118	0.0155
2-BTDA	2.55	2.52	0.0098	0.0129

the characteristic breakdown strength of the resulting PI films were summarized in Table 6. As a control, the commercially available DuPont Kapton 50HN PI film (thickness: 12.5 μm) was purchased and its breakdown strength was also measured under the same condition. The breakdown strength of the resulting PI films was between 461 and 523 kV mm^{-1}, which was higher than that of Kapton 50HN PI film (400 kV mm^{-1}). Besides, the distribution of the measured breakdown strength might be related to the heterogeneity in microstructure of films [60].

4. Conclusions

In summary, an asymmetric diamine **2** with a pedant bulky *m*-trifluoromethyl phenyl was synthesized and then polymerized with some commercially available aromatic dianhydrides to produce polyimides by the high-temperature one-pot polycondensation. Due to the introduction of bulky asymmetric fluorinated side groups, these resulting PIs possessed relatively large free volume and low polarizability, which endowed them low intrinsic *k* values in the range from 2.66 to 3.04 at 1 MHz and 2.38–2.87 at 10 GHz. Furthermore, these PI films also exhibited some better integrative properties, including high breakdown strength, moderate mechanical properties, excellent thermal stability, good optical transparency and solubility in organic solvents, which make them as promising candidates for the microelectronics field.

Declaration of Competing Interest

The author(s) declared no potential conflicts of interest with respect to the research, authorship, and/or publication of this article.

Acknowledgements

This work was supported by Science and Technology Commission of Shanghai Municipality Basic Research Project (No. 16JC1403600), Equipment Research and Development Sharing Technology Project (No. 41421060301).

Appendix A. Supplementary data

Supplementary data to this article can be found online at https://doi.org/10.1016/j.reactfunctpolym.2021.105065.

References

[1] P.P. Zhang, J.P. Zhao, K. Zhang, Y.Y. Wu, Y. Li, Effect of co-solvent on the structure and dielectric properties of porous polyimide membranes, J. Phys. D. Appl. Phys. 51 (2018) 215305, https://doi.org/10.1088/1361-6463/aabe19.
[2] N.N. Song, H.Y. Yao, T.N. Ma, T.J. Wang, K.X. Shi, Y. Tian, B. Zhang, S.Y. Zhu, Y. H. Zhang, S.W. Guan, Decreasing the dielectric constant and water uptake by introducing hydrophobic cross-linked networks into co-polyimide films, Appl. Surf. Sci. 480 (2019) 990–997, https://doi.org/10.1016/j.apsusc.2019.02.141.
[3] W.X. Chen, Z.X. Zhou, T.T. Yang, R.X. Bei, Y. Zhang, S.W. Liu, Z.G. Chi, X.D. Chen, J.R. Xu, Synthesis and properties of highly organosoluble and low dielectric constant polyimides containing non-polar bulky triphenyl methane moiety, React. Funct. Polym. 108 (2016) 71–77, https://doi.org/10.1016/j.reactfunctpolym.2016.04.011.
[4] R.X. Bei, C. Qian, Y. Zhang, Z.G. Chi, S.W. Liu, X.D. Chen, J.R. Xu, M.P. Aldred, Intrinsic low dielectric constant polyimides: relationship between molecular structure and dielectric properties, J. Mater. Chem. C 5 (2017) 12807–12815, https://doi.org/10.1039/C7TC04220E.
[5] M.C. Jia, M.T. Zhou, Y.J. Li, G.L. Lu, X.Y. Huang, Construction of semi-fluorinated polyimides with perfluorocyclobutyl aryl ether-based side chains, Polym. Chem. 9 (2018) 920–930, https://doi.org/10.1039/C8PY00004B.
[6] S.H. Han, Y.N. Li, F.Y. Hao, H. Zhou, S.L. Qi, G.F. Tian, D.Z. Wu, Ultra-low dielectric constant polyimides: combined efforts of fluorination and micro-

branched crosslink structure, Eur. Polym. J. 143 (2021) 110206, https://doi.org/10.1016/j.eurpolymj.2020.110206.
[7] Y.S. Zheng, L. Yu, Z.W. Wang, X.S. Chen, J. Li, Y. Zou, D.Y. Ji, L.Q. Li, W.P. Hu, Functionalization of low-*k* polyimide gate dielectrics with self-assembly monolayer toward high-performance organic field-effect transistors and circuits, Adv. Mater. Interfaces 8 (2021) 2100217, https://doi.org/10.1002/admi.202100217.
[8] C.P. Yang, R.S. Chen, K.H. Chen, Effects of diamines and their fluorinated groups on the color lightness and preparation of organosoluble aromatic polyimides from 2,2-bis 4-(4-amino-2-trifluoromethylphenoxy) phenyl-hexafluoropropane, J. Polym. Sci. A Polym. Chem. 41 (2003) 922–938, https://doi.org/10.1002/pola.10629.
[9] Y.W. Liu, Y. Zhang, Q. Lan, S.W. Liu, Z.X. Qin, L.H. Chen, C.Y. Zhao, Z.G. Chi, J. R. Xu, J. Economy, High-performance functional polyimides containing rigid nonplanar conjugated triphenylethylene moieties, Chem. Mater. 24 (2012) 1212–1222, https://doi.org/10.1021/cm3003172.
[10] M. Zhang, W.L. Liu, X. Gao, P. Cui, T. Zou, G.H. Hu, L.M. Tao, L. Zhai, Preparation and characterization of semi-alicyclic polyimides containing trifluoromethyl groups for optoelectronic application, Polymers 12 (2020) 1532, https://doi.org/10.3390/polym12071532.
[11] Y.C. Wu, Z.G. Chen, J.Q. Ji, Y.B. Zhou, H.H. Huang, S.M. Liu, J.Q. Zhao, Multifunctional polyimides by direct silyl ether reaction of pendant hydroxy groups: toward low dielectric constant, high optical transparency and fluorescence, Eur. Polym. J. 132 (2020) 109742, https://doi.org/10.1016/j.eurpolymj.2020.109742.
[12] Z.H. Pan, S.H. Han, J.H. Wang, S.L. Qi, G.F. Tian, D.Z. Wu, Polyimide fabric-reinforced polyimide matrix composites with excellent thermal, mechanical, and dielectric properties, High Perform. Polym. 32 (2020) 1085–1093, https://doi.org/10.1177/0954008320928387.
[13] G.R. Qiu, W.S. Ma, Y.Q. Jiao, L. Wu, Low-dielectric-constant aromatic homopolyimide and copolyimide derived from pyromellitic dianhydride, 4,4′-oxydianiline, 2,2-bis[4-(4-aminephenoxy)phenyl]propane, 1,4-bis(4-aminophenoxy)benzene, or 1,3-bis(4-aminophenoxy)benzene, J. Appl. Polym. Sci. 136 (2019) 47405, https://doi.org/10.1002/app.47405.
[14] L.Y. Pu, X. Huang, W. Wang, Y.T. Dai, J.X. Yang, H. Zhang, Strategy to achieve ultralow dielectric constant for polyimide: introduction of fluorinated blocks and fluorographene nanosheets by in situ polymerization, J. Mater. Sci.-Mater. Electron. 30 (2019) 14679–14686, https://doi.org/10.1007/s10854-019-01839-3.
[15] J.-W. Zha, H.-J. Jia, H.-Y. Wang, Z.-M. Dang, Tailored ultralow dielectric permittivity in high-performance fluorinated polyimide films by adjusting nanoporous characterisitics, J. Phys. Chem. C 116 (2012) 23676–23681, https://doi.org/10.1021/jp305286r.
[16] Z.L. Li, H.W. Zou, P.B. Liu, Morphology and properties of porous polyimide films prepared through thermally induced phase separation, RSC Adv. 5 (2015) 37837–37842, https://doi.org/10.1039/C5RA01514F.
[17] J.W. Li, G.C. Zhang, Q. Zhu, J.T. Li, H.M. Zhang, Z.X. Jing, Synthesis and properties of ultralow dielectric constant porous polyimide films containing trifluoromethyl groups, J. Appl. Polym. Sci. 134 (2017) 44494, https://doi.org/10.1002/app.44494.
[18] C. Wang, T.M. Wang, Q.H. Wang, Controllable porous fluorinated polyimide thin films for ultralow dielectric constant interlayer dielectric applications, J. Macromol. Sci. Part A-Pure Appl. Chem. 54 (2017) 311–315, https://doi.org/10.1080/10601325.2017.1294453.
[19] P.X. Lv, Z.X. Dong, X.M. Dai, X.P. Qiu, Flexible polydimethylsiloxane-based porous polyimide films with an ultralow dielectric constant and remarkable water resistance, ACS Appl. Polym. Mater. 1 (2019) 2597–2605, https://doi.org/10.1021/acsapm.9b00484.
[20] Y. Kourakata, T. Onodera, H. Kasai, H. Jinnai, H. Oikawa, Ultra-low dielectric properties of porous polyimide thin films fabricated by using the two kinds of templates with different particle sizes, Polymer 212 (2021) 123115, https://doi.org/10.1016/j.polymer.2020.123115.
[21] J.L. Hedrick, R.D. Miller, C.J. Hawker, K.R. Carter, W. Volksen, D.Y. Yoon, M. Trollsås, Templating nanoporosity in thin-film dielectric insulators, Adv. Mater. 10 (1998) 1049–1053, https://doi.org/10.1002/(SICI)1521-4095(199809)10:13<1049::AID-ADMA1049>3.0.CO;2-F.
[22] W. Chen, F.L. Liu, M. Ji, S.Y. Yang, Synthesis and characterization of low-CTE polyimide films containing trifluoromethyl groups with water-repellant characteristics, High Perform. Polym. 29 (2017) 501–512, https://doi.org/10.1177/0954008316650014.
[23] P.X. Lv, Z.X. Dong, X.M. Dai, H.F. Wang, X.P. Qiu, Synthesis and properties of ultralow dielectric porous polyimide films containing adamantane, J. Polym. Sci. A Polym. Chem. 56 (2018) 549–559, https://doi.org/10.1002/pola.28928.
[24] C. Yuan, K.K. Jin, K. Li, S. Diao, J.W. Tong, Q. Fang, Non-porous low-*k* dielectric films based on a new structural amorphous fluoropolymer, Adv. Mater. 25 (2013) 4875–4878, https://doi.org/10.1002/adma.201302021.
[25] C.D. Simone, E. Vaccaro, D.A. Scola, The synthesis and characterization of highly fluorinated aromatic polyimides, J. Fluor. Chem. 224 (2019) 100–112, https://doi.org/10.1016/j.jfluchem.2019.05.001.
[26] Z.Q. Wang, M.Y. Zhang, E.L. Han, H.Q. Niu, D.Z. Wu, Structure-property relationship of low dielectric constant polyimide fibers containing fluorine groups, Polymer 206 (2020) 122884, https://doi.org/10.1016/j.polymer.2020.122884.
[27] T. Zhang, Y. Pan, C. Song, B. Huang, Z.-Z. Huang, High optical transparency, low dielectric constant and light color of organosoluble fluorinated polyimides based on 10,10-bis[4-(4-amino-3-trifluoromethylphenoxy)phenyl]-9(*10H*)-anthrone, Polym. Bull. 77 (2020) 4077–4094, https://doi.org/10.1007/s00289-019-02955-0.
[28] Y.W. Liu, Y. Zhang, Q. Lan, Z.X. Qin, S.W. Liu, C.Y. Zhao, Z.G. Chi, J.R. Xu, Synthesis and properties of high-performance functional polyimides containing rigid nonplanar conjugated tetraphenylethylene moieties, J. Polym. Sci. A Polym. Chem. 51 (2013) 1302–1314, https://doi.org/10.1002/pola.26498.
[29] Y.W. Liu, Z.X. Zhou, L.J. Qu, B. Zou, Z.Q. Chen, Y. Zhang, S.W. Liu, Z.G. Chi, X. D. Chen, J.R. Xu, Exceptionally thermostable and soluble aromatic polyimides with special characteristics: intrinsic ultralow dielectric constant, static random access memory behaviors, transparency and fluorescence, Mater. Chem. Front. 1 (2017) 326–337, https://doi.org/10.1039/C6QM00027D.
[30] C. Qian, R.X. Bei, T.W. Zhu, W.W. Zheng, S.W. Liu, Z.G. Chi, M.P. Aldred, X. D. Chen, Y. Zhang, J.R. Xu, Facile strategy for intrinsic low-*k* dielectric polymers: molecular design based on secondary relaxation behavior, Macromolecules 52 (2019) 4601–4609, https://doi.org/10.1021/acs.macromol.9b00136.
[31] Y.-W. Liu, L.-S. Tang, L.-J. Qu, S.-W. Liu, Z.-G. Chi, Y. Zhang, J.-R. Xu, Synthesis and properties of high performance functional polyimides containing rigid nonplanar conjugated fluorene moieties, Chin. J. Polym. Sci. 37 (2019) 416–427, https://doi.org/10.1007/s10118-019-2225-0.
[32] Y.W. Liu, C. Qian, L.J. Qu, Y.N. Wu, Y. Zhang, X.H. Wu, B. Zou, W.X. Chen, Z. Q. Chen, Z.G. Chi, S.W. Liu, X.D. Chen, J.R. Xu, A bulk dielectric polymer film with intrinsic ultralow dielectric constant and outstanding comprehensive properties, Chem. Mater. 27 (2015) 6543–6549, https://doi.org/10.1021/acs.chemmater.5b01798.
[33] Q. Wu, X.R. Ma, F. Zheng, X.M. Lu, Q.H. Lu, High performance transparent polyimides by controlling steric hindrance of methyl side groups, Eur. Polym. J. 120 (2019) 109235, https://doi.org/10.1016/j.eurpolymj.2019.109235.
[34] Y.-T. Chern, J.-Y. Tsai, Low dielectric constant and high organosolubility of novel polyimide derived from unsymmetric 1,4-bis(4-aminophenoxy)-2,6-di-*tert*-butylbenzene, Macromolecules 41 (2008) 9556–9564, https://doi.org/10.1021/ma802305q.
[35] S. Bong, H. Yeo, B.-C. Ku, M. Goh, N.-H. You, Highly soluble polyimide based on asymmetric diamines containing trifluoromethyl group for high performance dielectric material, Macromol. Res. 26 (2018) 85–91, https://doi.org/10.1007/s13233-018-6010-7.
[36] G. Socrates, Infrared and Raman Characteristic Group Fregueneies, 3rd ed., John Wiley & Sons Ltd, Chichester, 2001.
[37] K.U. Jeong, Y.-J. Jo, T.-H. Yoon, Synthesis and characterization of novel polyimide from bis-(3-aminophenyl)-4-(trifluoromethyl)phenyl phosphine oxide, J. Polym. Sci. A Polym. Chem. 39 (2001) 3335–3347, https://doi.org/10.1002/pola.1316.
[38] L. Yi, C.Y. Li, W. Huang, D.Y. Yan, Soluble polyimides from 4,4′-diaminodiphenyl ether with one or two *tert*-butyl pedant groups, Polymer 80 (2015) 67–75, https://doi.org/10.1016/j.polymer.2015.10.045.
[39] Z.-H. Wang, H.-X. Yang, S.-Y. Yang, Quartz fiber cloth-reinforced semi-aromatic thermosetting polyimide composite with high-frequency low dielectric constant, High Perform. Polym. 32 (2020) 91–102, https://doi.org/10.1177/0954008319853028.
[40] Y.B. Zhuang, J.G. Seong, Y.S. Do, W.H. Lee, M.J. Lee, M.D. Guiver, Y.M. Lee, High-strength, soluble polyimide membranes incorporating Tröger's base for gas separation, J. Membr. Sci. 504 (2016) 55–65, https://doi.org/10.1016/j.memsci.2015.12.057.
[41] Y.X. Feng, J.Z. Ren, H. Li, D. Zhao, L.J. Sheng, Y.D. Wu, W.Y. Zhao, M. Deng, Effect of thermal annealing on gas separation performance and aggregation structures of block polyimide membranes, Polymer 219 (2021) 123538, https://doi.org/10.1016/j.polymer.2021.123538.
[42] M. Calle, A.E. Lozano, J. de Abajo, J.G. de la Campa, C. Álvarez, Design of gas separation membranes derived of rigid aromatic polyimides. 1. Polymers from diamines containing di-*tert*-butyl side groups, J. Membr. Sci. 365 (2010) 145–153, https://doi.org/10.1016/j.memsci.2010.08.051.
[43] M.J. Hou, W.B. Qi, L. Li, R.S. Xu, J.J. Xue, Y.Y. Zhang, C.W. Song, T.H. Wang, Carbon molecular sieve membrane with tunable microstructure for CO_2 separation: effect of multiscale structures of polyimide precursors, J. Membr. Sci. 635 (2021) 119541, https://doi.org/10.1016/j.memsci.2021.119541.
[44] Y.W. Liu, A. Tang, J.H. Tan, C.L. Chen, D. Wu, H.L. Zhang, Structure and gas barrier properties of polyimide containing a rigid planar fluorene moiety and an amide group: insights from molecular simulations, ACS Omega 6 (2021) 4273–4281, https://doi.org/10.1021/acsomega.0c05278.
[45] D.-J. Liaw, W.-T. Tseng, New organosoluble polyimides with low dielectric constants derived from bis[4-(2-trifluoromethyl-4-aminophenoxy)phenyl] diphenylmethylene, Macromol. Symp. 199 (2003) 351–362, https://doi.org/10.1002/masy.200350930.
[46] K. Goto, Y. Inoue, M. Matsubara, Low dielectric and thermally stable polyimides with fluorene structure (II) relationship between chemical structure and dielectric constant, J. Photopolym. Sci. Technol. 14 (2001) 33–36, https://doi.org/10.2494/photopolymer.14.33.
[47] P.K. Tapaswi, C.-S. Ha, Recent trends on transparent colorless polyimides with balanced thermal and optical properties: design and synthesis, Macromol. Chem. Phys. 220 (2019) 1800313, https://doi.org/10.1002/macp.201800313.
[48] Q. Wu, X.R. Ma, F. Zheng, X.M. Lu, Q.H. Lu, Synthesis of highly transparent and heat-resistant polyimides containing bulky pendant moieties, Polym. Int. 68 (2019) 1186–1193, https://doi.org/10.1002/pi.5811.
[49] K.-M. Jeong, P.K. Tapaswi, T. Kambara, R. Ishige, S. Ando, C.-S. Ha, Photoconductive polyimides derived from a novel imidazole-containing diamine, High Perform. Polym. 32 (2020) 620–630, https://doi.org/10.1177/0954008319892307.
[50] X.Q. He, S.B. Wang, X.M. Wu, C. Shu, X. Fan, Z.H. Yu, W. Huang, Soluble and transparent polyimides with high T_gs from a new semi-aliphatic diamine with

cyclohexyl and ortho-methyl groups, High Perform. Polym. 33 (2021) 528–537, https://doi.org/10.1177/0954008320967052.
[51] H. Yeo, M. Goh, B.-C. Ku, N.-H. You, Synthesis and characterization of highly-fluorinated colorless polyimides derived from 4,4′-((perfluoro-[1,1′-biphenyl]-4,4′-diyl)bis(oxy))bis(2,6-dimethylaniline) and aromatic dianhydrides, Polymer 76 (2015) 280–286, https://doi.org/10.1016/j.polymer.2015.09.019.
[52] L. Yi, C.Y. Li, W. Huang, D.Y. Yan, Soluble and transparent polyimides with high T_g from a new diamine containing *tert*-butyl and fluorene units, J. Polym. Sci. A Polym. Chem. 54 (2016) 976–984, https://doi.org/10.1002/pola.27933.
[53] S. Ando, T. Matsuura, S. Sasaki, Coloration of aromatic polyimides and electronic properties of their source materials, Polym. J. 29 (1997) 69–76, https://doi.org/10.1295/polymj.29.69.
[54] A.I. Barzic, C. Hulubei, M. Asandulesa, G. Lisa, D. Popovici, I. Stoica, A. Nicolescu, R.M. Albu, Interlayer dielectrics based on copolyimides containing non-coplanar alicyclic-units for multilevel high-speed electronics, Polym. Test. 90 (2020) 106704, https://doi.org/10.1016/j.polymertesting.2020.106704.
[55] Y.H. Zhang, L. Yu, Q.S. Su, H. Zheng, H.T. Huang, H.L.W. Chan, Fluorinated polyimide-silica films with low permittivity and low dielectric loss, J. Mater. Sci. 47 (2012) 1958–1963, https://doi.org/10.1007/s10853-011-5990-x.
[56] H.-T. Zuo, F. Gan, J. Dong, P. Zhang, X. Zhao, Q.-H. Zhang, Highly transparent and colorless polyimide film with low dielectric constant by introducing *meta*-substituted structure and trifluoromethyl groups, Chin. J. Polym. Sci. 39 (2021) 455–464, https://doi.org/10.1007/s10118-021-2514-2.
[57] W. Jang, D. Shin, S. Choi, S. Park, H. Han, Effects of internal linkage groups of fluorinated diamine on the optical and dielectric properties of polyimide thin films, Polymer 48 (2007) 2130–2143, https://doi.org/10.1016/j.polymer.2007.02.023.
[58] A. Iqbal, S.H. Lee, H.M. Siddiqi, O.O. Park, T. Akhter, Enhanced dielectric constant, ultralow dielectric loss, and high-strength imide-functionalized graphene oxide/hyperbranched polyimide nanocomposites, J. Phys. Chem. C 122 (2018) 6555–6565, https://doi.org/10.1021/acs.jpcc.8b00493.
[59] L. Li, N. Bowler, P.R. Hondred, M.R. Kessler, Statistical analysis of electrical breakdown behavior of polyimide following degrading processes, IEEE Trns. Dielectr. Electr. Insul. 18 (2011) 1955–1962, https://doi.org/10.1109/TDEI.2011.6118633.
[60] R. Ma, A.F. Baldwin, C.C. Wang, I. Offenbach, M. Cakmak, R. Ramprasad, G. A. Sotzing, Rationally designed polyimides for high-energy density capacitor applications, ACS Appl. Mater. Interfaces 6 (2014) 10445–10451, https://doi.org/10.1021/am502002v.